A Compact Photomicroreactor Design for Kinetic Studies of Gas-Liquid Photocatalytic Transformations

Yuanhai Su and Volker Hessel
Micro Flow Chemistry and Process Technology, Dept. of Chemical Engineering and Chemistry, Eindhoven University of Technology, Den Dolech 2, 5600 MB Eindhoven, The Netherlands

Timothy Noël
Micro Flow Chemistry and Process Technology, Dept. of Chemical Engineering and Chemistry, Eindhoven University of Technology, Den Dolech 2, 5600 MB Eindhoven, The Netherlands

Dept. of Organic Chemistry, Ghent University, Krijgslaan 281 (S4), 9000 Gent, Belgium

DOI 10.1002/aic.14813
Published online April 9, 2015 in Wiley Online Library (wileyonlinelibrary.com)

A compact photomicroreactor assembly consisting of a capillary microreactor and small-scale light emitting diodes was developed for the study of reaction kinetics in the gas-liquid photocatalytic oxidation of thiophenol to phenyl disulfide within Taylor flow. The importance of photons was convincingly shown by a suction phenomenon due to the fast consumption of oxygen. Mass transfer limitations were evaluated and an operational zone without mass transfer effects was chosen to study reaction kinetics. Effects of photocatalyst loading and light sources on the reaction performance were investigated. Reaction kinetic analysis was performed to obtain reaction orders with respect to both thiophenol and oxygen based on heterogeneous and homogeneous experimental results, respectively. The Hatta number further indicated elimination of mass transfer limitations. Reaction rate constants at different photocatalyst loadings and different photon flux were calculated. Furthermore, the advantages of this photomicroreactor assembly for studying gas-liquid photocatalytic reaction kinetics were demonstrated as compared with batch reactors. © 2015 American Institute of Chemical Engineers *AIChE J*, 61: 2215–2227, 2015

Keywords: microreactors, photocatalysis, disulfides, aerobic oxidation, mass transfer, reaction kinetics

Introduction

Photochemical transformations are commonly used in the fields of organic synthesis, material science, and environmental treatment.[1–5] In these applications, photons are utilized to provide sufficient energy to overcome the activation barrier. Light activation provides remarkable pathways for many kinds of reactions, which are difficult or impossible to reach via thermochemical activation. The reactant molecules can be excited by either direct or indirect excitation. In the direct excitation, the reactant molecules should contain a chromophoric moiety which can absorb light energy efficiently. This direct excitation is often restricted to UV photochemistry. As compared with direct excitation, indirect excitation provides higher application potential for photochemical processes, in which incident light is absorbed by a photocatalyst or photosensitizer. Next, the electrons or energy are transferred to acceptor molecules which undergo subsequent transformations. Recently, the use of visible light photoredox catalysis has become very popular in organic synthetic chemistry as it allows to perform chemical reactions under mild reaction conditions (For selected reviews of visible light photoredox catalysis, see Refs. 6–8).

Immersion-well photoreactors in conjunction with mercury-vapor discharge lamps are an outstanding representative of photoreactors, and they are widely used for UV photochemical transformations in organic synthetic laboratories.[9] However, the mixing efficiency, heat and mass transfer rates in these batch reactors are usually insufficient especially for fast photochemical reactions. Moreover, it is difficult to reach a homogeneous irradiation inside batch reactors due to their large characteristic dimensions. This photon maldistribution originates from long transport distance according to the Bouguer-Lambert-Beer law.[9,10] The larger the dimensions of batch reactors are, the more pronounced the attenuation effect of photon transport becomes in photochemical processes. This makes the scale-up of batch reactors via a dimension enlarging approach very challenging. In addition, safety risks are associated with some photochemical processes carried out in batch reactors, such as aerobic oxidations,[11–14] and reactions involving the use of toxic and hazardous materials, for example, diazonium salts[15] and azides.[16]

These limitations may be overcome by utilizing microreactor technology as it offers several advantages, such as continuous-flow operation, large specific surface area,

Additional Supporting Information may be found in the online version of this article.

Correspondence concerning this article should be addressed to T. Noël at t.noel@tue.nl.

© 2015 American Institute of Chemical Engineers

enhanced heat and mass transfer rates, reduced safety hazards, and the ease of increasing throughput by numbering-up.[17–24] Furthermore, extremely small characteristic dimensions of microreactors ensure excellent light irradiation of the entire reaction medium and thus provide an irradiation homogeneity, resulting in higher reaction selectivity, shorter reaction times, and lower catalyst loadings.[25–29] Microreactors have been extensively applied for various gas-liquid photochemical processes, such as cycloadditions,[30–32] trifluoromethylations,[33,34] and singlet oxygen oxidations.[35,36]

Lévesque and Seeberger[11] developed a transparent capillary microreactor for the aerobic oxidation of citronellol, which was coiled around a 450 W medium-pressure mercury lamp with a controlled temperature (25°C). Tetraphenylporphyrin (TPP) was used as a photocatalyst, and different reaction parameters (such as pressure, stoichiometry, and concentration of TPP) were rapidly screened within Taylor flow. A variety of substrates could be oxidized in short reaction times (0.8–1.3 min), with excellent scalability and stability of this photocatalytic process. Singlet oxygen could be easily generated in a falling film microreactor with the illumination of a Xenon lamp, and then used for the [4+2] cycloaddition of cyclopentadiene.[37] This microreactor design provides 32 parallel microchannels inside which liquid films with a thickness of about 20 μm were formed when the oxygen and the liquid phase were brought to contact, resulting in high specific interfacial area up to 20,000 m^2m^{-3} leading to 20% yield of the desired compound at short reaction times. Meyer et al.[38] compared the different reaction performance in an immersion-well photoreactor and a microreactor in terms of space-time yield and photonic efficiency. The oxidation of citronellol by singlet oxygen generated with the aid of a photosensitizer (ruthenium polypyridyl complex) was chosen as a model reaction, and light emitting diodes (LEDs) were used to illuminate the reaction mixture. Their results showed that the photonic efficiency in the microreactor was about two times larger than in immersion-well photoreactors, and the space-time yield was about one order of magnitude higher. Elvira et al.[39] designed a micro capillary film reactor consisting of a plastic film with multiple parallel channels, which provided a numbering-up strategy for the singlet oxygen mediated synthesis of ascaridole. The production rate of ascaridole was found to be strongly dependent on the partial pressure of oxygen present within the reaction system. As they claimed, this numbering-up strategy significantly simplified the reactor design, allowing for increased operation safety, and providing a space-time yield over 20 times larger than the batch processing.

To generate new, more efficient photocatalysts, and optimized chemical formulations, fundamental knowledge has to be gained on the reaction mechanism and corresponding kinetic characteristics. Chemical reaction kinetics is of significant importance for reactor design and process optimization, and can be classified as intrinsic and apparent kinetics.[40] The major advantage of intrinsic kinetics is that it is scale independent, in contrast with the apparent kinetics which includes the effects of transport phenomena. Due to excellent transport properties, microreactors have received increasing attention for the investigation of reaction kinetics in gas-liquid heterogeneous processes. Ye et al.[41] studied the influencing parameters on the CO_2 absorption by monoethanolamine solution and its apparent reaction kinetics via a microchannel reactor without evaluation of mass transfer limitation. Li et al.[42] developed a strategy to measure the kinetics of fast reactions of CO_2 with secondary amines within Taylor flow in a microfluidic system through a high speed camera system. This strategy relied on the microfluidic generation of highly monodisperse gas bubbles (Taylor bubbles) in the liquid reaction medium and subsequent analysis of time-dependent changes in bubble dimensions. The elimination of mass transfer limitations in reaction processes was confirmed by the increase in the consumption rate of CO_2 with increasing concentrations of absorbent. Keybl and Jensen[43] fabricated a silicon microreactor system which was capable of studying gas-liquid homogeneous catalysis at high temperature and high pressure. The hydroformylation of 1-octene was investigated within Taylor flow in this microreactor system, with both online and offline analysis using attenuated total reflectance Fourier transform infrared spectroscopy and gas chromatography (GC). Kinetic parameters of this reaction were determined by varying the pressure, temperature, and concentrations of both gas and liquid phases. The authors confirmed that the mass transfer limitation was eliminated by estimating the concentration gradient of carbon monoxide in the liquid phase. However, the application of microreactors for studying the reaction kinetics of gas-liquid photocatalytic processes has not been performed yet.

In this work, we designed and fabricated a compact photomicroreactor assembly that consisted of a capillary microreactor and LEDs for the study of gas-liquid photocatalytic processes. As a model reaction, we investigated the metal-free photocatalytic aerobic oxidation of thiophenol to phenyl disulfide under visible light illumination, which was recently developed in our group (see reaction equation R1).[44] Organic disulfides are important molecular and structural features in various biologically active compounds and fine chemicals.[45] Their application potential ranges from anti-oxidants, pharmaceuticals, agrochemicals, to vulcanizers. Optimized reaction conditions involved the use of Eosin Y as a metal-free photocatalyst and tetramethylethylenediamine (TMEDA) as a base. Ethanol was the optimal solvent for this transformation. Mass transfer limitations were evaluated by varying the volumetric flow rate ratio of the gas phase to the liquid phase, and its elimination was confirmed by comparing the concentration of oxygen in the liquid phase and the equilibrium concentration in the absence of any reaction. Next, the effects of photocatalyst concentration and LED light sources on the photocatalytic performance were studied without mass transfer limitation. Reaction kinetic analysis was performed, and the reaction orders with respect to both thiophenol and oxygen were deduced. The reaction rate constants at different photocatalyst loadings and different photon flux were calculated. Furthermore, the reaction rate constants obtained in the capillary microreactor were compared with those obtained in a batch reactor

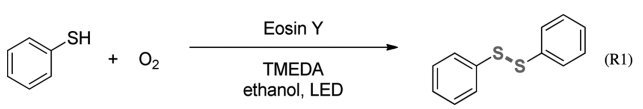

(R1)

Experimental

Photomicroreactor assembly design

In order to closely integrate the light sources and the capillary microreactor, commercial light stripes with small-scale LEDs (Paulmann Lighting GmbH) were used in the experiments. A transparent capillary made of high purity

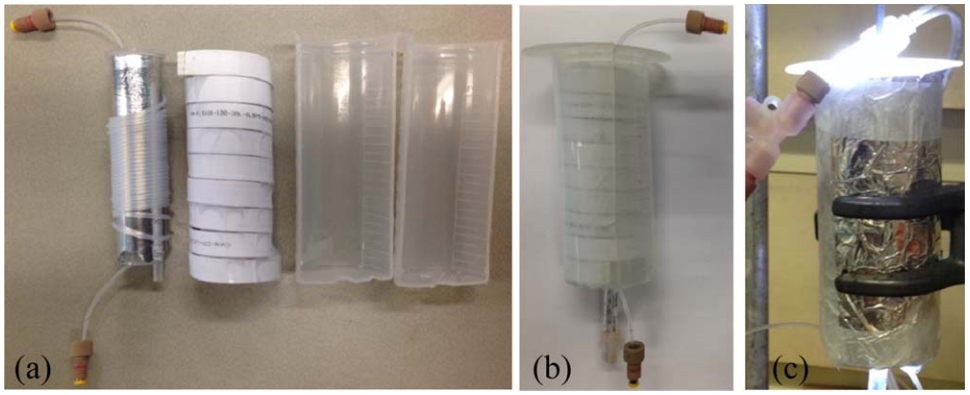

Figure 1. Photomicroreactor design.

(a) Different components of the photomicroreactor assembly, with (from left to right) the capillary microreactor coiled around an aluminum coated syringe, the LED stripe, and the outer syringe in which the photomicroreactor and LEDs are placed; (b) Assembled version; (c) Photomicroreactor assembly in operation. [Color figure can be viewed in the online issue, which is available at wileyonlinelibrary.com.]

perfluoroalkoxy alkane (PFA from IDEX Health and Science, transmission of 91–96% for visible light with wavelength of 400–700 nm; ID: 750 μm; length: 2.15 m; volume: 0.95 mL) was coiled around the outer wall of a 20 mL plastic syringe, which was coated with aluminum foil to refract the photons toward the reactor (see Figure 1). A LED stripe was coiled around the inner wall of a larger plastic syringe (100 mL), with all LED pillars (3 mm width and 2.5 mm height for each pillar) facing toward the central axis of this syringe. The syringe coiled with the capillary was fixed inside a larger diameter syringe. Consequently, a narrow gap between the LED pillars and the coiled capillary was ensured. In order to reduce the illumination loss, aluminum foil was fixed around the outer wall of the larger syringe. Furthermore, pressurized air was supplied through the nozzle of the larger syringe in order to keep the whole system at room temperature (22 ± 1°C), which could be detected by a thermocouple. Figure 1 shows the establishing process of this small photochemical column for the study of photochemical transformations and corresponding reaction kinetics. It is worth mentioning that the whole design of this photochemical column is based on cheap commercially available parts and common laboratory disposables. The total cost price of the photochemical column is below 100 euro and can be readily assembled within 30 min. Consequently, our design allows for a rapid implementation of this technology in any chemical laboratory.

Three different LED stripes (light sources 1–3) were applied to study the effects of light sources on photocatalytic transformations. The widths of all these LED stripes were 10 mm. Light sources 1–3 with different lengths (97 cm, 97 cm, and 100 cm) emitted white, warm white, and neon green light, respectively. The number of LED pillars along each stripe of light sources 1 and 2 was 39, and 30 LEDs for light source 3. An integrating sphere equipped with a Labsphere LPS 100-0260 light detector array was used to specify the emission spectral flux graph for these three LED light sources (shown in Figure 2a). The UV-VIS absorption spectrum of Eosin Y in the presence of TMEDA is also shown in the same figure (Figure 2b).

Experimental procedure

Schematic representation of the experimental setup and a picture of the small photochemical column under operation are shown in Figure 3. The substrate solution consisted of

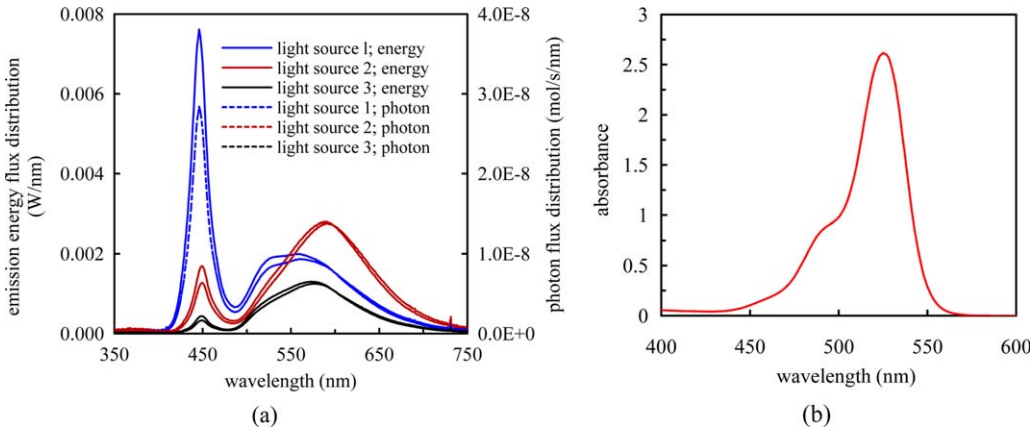

Figure 2. (a) Energy flux distribution and corresponding photon flux distribution per wavelength gap for three LED light sources; (b) UV-VIS absorption spectrum of Eosin Y with TMEDA in ethanol (25 μM Eosin Y and 2.5 mM TMEDA).

[Color figure can be viewed in the online issue, which is available at wileyonlinelibrary.com.]

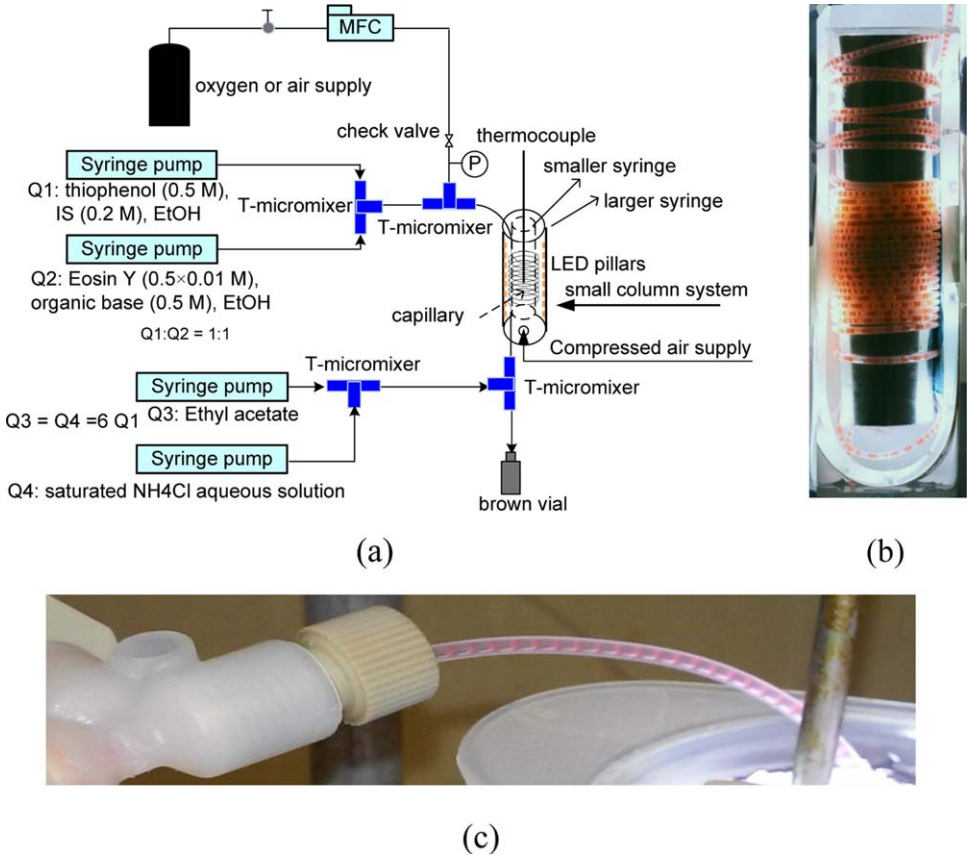

Figure 3. (a) Schematic representation of experimental setup; (b) A picture of an opening photochemical column system under Taylor flow running with a special treatment of LED stripe position; (c) gas-liquid Taylor flow in the capillary microreactor ($Q_1 = Q_2 = 50$ μL/min, $Q_g = 200$ μL/min).

[Color figure can be viewed in the online issue, which is available at wileyonlinelibrary.com.]

0.5 M thiophenol in ethanol with an internal standard (IS = α,α,α-trifluorotoluene) for GC analysis. This substrate solution was stored under argon atmosphere prior to reaction. No conversion of thiophenol could be found even when the storing time was more than 20 days. The catalyst solution consisted of Eosin Y, TMEDA and ethanol as the solvent. The substrate solution and the catalyst solution were introduced into the system by two syringe pumps (Fusion 200 Classic), merged in a T-micromixer (Tefzel® tee mixer with ID of 500 μm) and mixed in a short capillary (ID = 750 μm). The reaction mixture was next delivered to a second T-micromixer and contacted with oxygen controlled by a gas mass flow controller (Bronkhorst). A Taylor flow regime was established (Figure 3c), and then flowed through the capillary microreactor in the small photochemical column. A pressure transducer (Huba Control) was connected to the gas line in order to measure the pressure drop in the capillary microreactor, which could be used to calculate the residence time (t) of the gas-liquid two phases. In order to completely quench the reactions after exiting the capillary microreactor, aqueous ammonium chloride solution, and ethyl acetate were fed to a third T-micromixer and contacted with the gas-liquid biphasic stream from the photochemical column. After attaining a steady state regime, a small brown vial was used to collect the reaction mixture, where the aqueous and organic phases formed a clear interface. The organic phase in the brown vial was collected and analyzed by GC FID in order to obtain the product yield (Y = GC yield).

Results and Discussion

Evaluation of mass transfer limitation

It is well known that gas-liquid Taylor flow in microchannels and microcapillaries can provide high mass transfer rates for reaction processes. This flow pattern is characterized by elongated gas bubbles, which are separated from each other by liquid slugs and surrounded by thin liquid films.[46,47] The increased gas-liquid interfacial area due to the segmentation and the internal circulations in the liquid slugs both give rise to fast mass transfer between gas-liquid two phases.[48–50] Furthermore, there exists a competition between mass transfer and chemical reactions in fast gas-liquid reactions. A dimensionless parameter, that is Hatta number (*Ha*), is usually used to determine whether mass transfer dominates the gas-liquid heterogeneous reaction proces.[51,52] *Ha* compares the rate of reaction in the liquid film (gas-liquid interfacial zone) to the rate of diffusion through the liquid film. The mass transfer will play an important role in reaction processes when *Ha* is larger than a certain value (e.g., $Ha > 3$). However, this method based on Hatta number for predicting the effect of mass transfer on reaction processes is not feasible when the reaction kinetic parameters are not available.

In the aerobic oxidation of thiophenol, the reaction process was varied from a very sluggish to fast reaction under photoredox catalysis (Eosin Y in the presence of TMEDA as a catalytic system). This could be well demonstrated by the suction phenomenon observed in the capillary microreactor

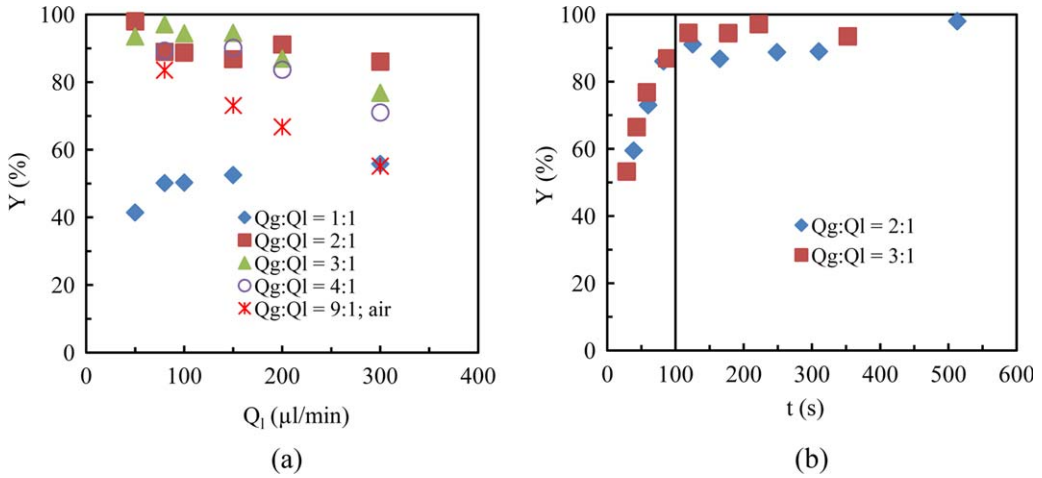

Figure 4. Effect of volumetric flow rate ratio of gas phase to liquid phase on the yield of phenyl disulfide (condition: 1 mol% Eosin Y loading, 1 equivalent TMEDA and light source 1).

(a) The relationship between the yield and the liquid phase flow rate; (b) the relationship between the yield and the residence time at two different volumetric flow rate ratios of gas phase to liquid phase. [Color figure can be viewed in the online issue, which is available at wileyonlinelibrary.com.]

(see video in Supporting Information), which resulted from the fast oxygen consumption under photocatalysis. In this suction process, oxygen was quickly consumed after turning on the LED light and a negative pressure was formed inside the capillary microreactor, resulting in an inverse flow of the gas-liquid two phases. After a period of LED light illumination, the hydrodynamics of gas-liquid two phases in the capillary microreactor reached steady state and the suction phenomenon disappeared. The suction phenomenon indicates the importance of the mass transfer rate (or supply) of oxygen and the light irradiation during this photocatalytic aerobic oxidation of thiophenol.

Figure 4 shows the effect of the volumetric flow rate ratio of gas phase to liquid phase on the yield of phenyl disulfide at different liquid phase flow rates. As shown in Figure 4a, an increase in the volumetric flow rate ratio of gas to liquid phase from 1 to 2 or to higher values resulted in higher yield at the same liquid phase flow rates when using pure oxygen as the gas phase. The increase in volumetric flow rate ratio reduced the residence time of reaction mixture in the capillary microreactor. Nevertheless, it shortened the length of the liquid slugs in the capillary microreactor, which intensified the internal circulations inside the liquid slugs and increased the interfacial area. Consequently, this leads to an enhanced mass transfer between the gas and liquid phases. The supply of oxygen for the photocatalytic process was not sufficient when the volumetric flow rate ratio was 1. This could be confirmed by the experimental observation that the presence of gas bubbles was absent in the effluent from the capillary microreactor. When the volumetric flow rate ratio reached 2, the mole ratio of oxygen to thiophenol was 0.33. A further increase in the volumetric flow rate ratio did not improve the yield due to the shorter residence time. In addition, the yield significantly decreased when pure oxygen was replaced by air, while keeping the mole ratio of oxygen to thiophenol constant (0.33). This can be attributed to the decreased mass transfer driving force between the gas phase and the liquid phase. In contrast, the mass transfer driving force was much higher when pure oxygen was used. The mass transfer resistance only existed in the gas-liquid interface and in the liquid phase in the case of introducing pure oxygen. Moreover, the residence time was much shorter when using air.

When the volumetric flow rate ratio reached 2, the mass transfer limitation of oxygen was totally eliminated at high flow rates (i.e., short residence times). As shown in Figure 4b, the yield did not depend on the volumetric flow rate ratio when the residence time was less than 100 s. The residence time was calculated based on Eq. 1, in which the oxygen consumption and the pressure drop across the capillary microreactor in the photochemical column were considered. In the following study of reaction kinetics, the operational zone without the mass transfer limitation (cf., Zone 1 in Figure 4b) and the volumetric flow rate of gas to liquid phase of 3 were chosen

$$t=\frac{V_c}{Q_G+Q_L}=\frac{V_c}{\frac{Q_{G,in}+Q_{G,out}}{2}\times\frac{P_{out}}{(P_{in}+P_{out})/2}+Q_L}$$
$$=\frac{V_c}{\frac{Q_{G,in}+(Q_{G,in}-0.25Q_LC_{sub,0}RTY/P_{out})}{2}\times\frac{P_{out}}{(P_{in}+P_{out})/2}+Q_L} \quad (1)$$

where V_c is the volume of capillary microreactor, $Q_{G,in}$ and $Q_{G,out}$ are the inlet and outlet volumetric flow rates of gas phase based on the atmospheric pressure, P_{in} and P_{out} are the inlet and outlet pressures in the capillary microreactor, and Q_L is the volumetric flow rate of liquid phase, $C_{sub,0}$ is the original concentration of thiophenol in the reaction mixture, R is the gas constant, and T is the reaction temperature. Based on the knowledge of hydrodynamics and mass transfer for Taylor flow in microchannels or in capillaries[53–55] and the physical properties (e.g., D_{O_2}, diffusivity of oxygen in ethanol), we can approximately calculate the concentration of oxygen in the liquid phase in this photocatalytic process. For example, the liquid side volumetric mass transfer coefficient (k_La) is about 1 s^{-1} when the flow rates of gas and liquid phase are 900 μL/min and 300 μL/min ($t = 58$ s) respectively. According to the mass balance of oxygen, the following equation can be obtained

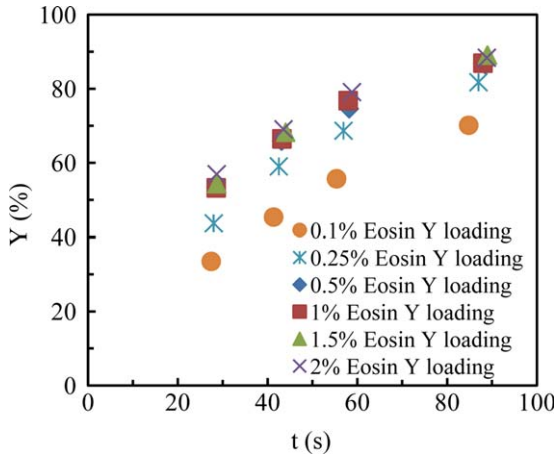

Figure 5. Effect of Eosin Y loading amount on the yield (1 equivalent TMEDA and light source 1).

[Color figure can be viewed in the online issue, which is available at wileyonlinelibrary.com.]

$$r_{O_2} = -\frac{dC_{O_2,L}}{dt} = -\frac{1}{4}\frac{dC_{sub}}{dt} = -\frac{1}{4}\frac{\Delta C_{sub}}{t} = k_L a(C_{O_2,in} - C_{O_2,L}) = k_L a(C^*_{O_2} - C_{O_2,L}) = 0.00082\,M/s \quad (2)$$

where $C^*_{O_2}$, $C_{O_2,in}$, and $C_{O_2,L}$ are the saturated concentration of oxygen (0.0098 M) in the ethanol, the interfacial concentration of oxygen between the gas-liquid two phases and the actual concentration of oxygen in the bulk liquid phase, respectively. The interfacial concentration is considered to be equal to the saturated concentration based on the assumption that the oxygen concentration reaches an equilibrium state at the gas-liquid interface. Consequently, the following equation can be deduced based on Eq. 2

$$\frac{C^*_{O_2} - C_{O_2,L}}{C^*_{O_2}} = \frac{0.00082\,M/s}{C^*_{O_2} k_L a} = 8\% \quad (3)$$

According to Eq. 3, the relative deviation between the saturated concentration and the actual concentration of oxygen in the bulk liquid phase is not more than 8%. Consequently, the oxygen concentration in the bulk liquid phase can be considered to reach the saturated state. These results further demonstrated the elimination of mass transfer limitation within the proper operational zone (Zone 1) of Taylor flow in the capillary microreactor for this gas-liquid two-phase photocatalytic process.

Influencing factors of photocatalytic aerobic oxidation

Effect of Photocatalyst (Eosin Y) Loading. The presence of Eosin Y is crucial for the photocatalytic aerobic oxidation. The absorption of visible light by Eosin Y initiates the photochemical process via a single electron transfer event.[56] Figure 5 shows the effect of the Eosin Y loading (φ, molar percentage) on the yield, with using light source 1. As expected, the yield increased with increasing amounts of Eosin Y. It was found that 0.5% of Eosin Y was optimal. A further increase of the Eosin Y loading did not lead to an improvement in yield. This can be probably attributed to photon transport limitations and higher catalyst loadings would require higher photon fluxes.

Effect of LED Light Sources. One of the most important factors in photoredox catalysis is the irradiative electronic energy transfer, which mainly depends on the spectral overlap integral, the photocatalyst concentration, the absorption path length, and the quantum efficiency. As is evident from Figure 2a, all three different LED light sources could emit the appropriate wavelength for excitation of Eosin Y (Figure 2b). Figure 6 compares the reaction performance for these three LED light sources at two different Eosin Y loadings. It can be seen that the yield was higher with light source 1 than with light sources 2 and 3. This is attributed to the higher light intensity (photon flux) emitted by light source 1 with a maximum emission in the range of 440– 560 nm (Figure 2a). Unexpectedly, the reaction performance with 1% Eosin Y loading was the same as with 0.25% Eosin loading for light source 3, as shown in Figure 7. The emission intensity in the range of 440–560 nm was rather low for light source 3. Even at relatively low photocatalyst concentration (e.g., 0.25% loading), the reaction mixture could effectively absorb the light emission from light source 3. This finding clearly demonstrates that it is essential to match the photon flux emitted by the light source with the concentration of the photocatalyst.

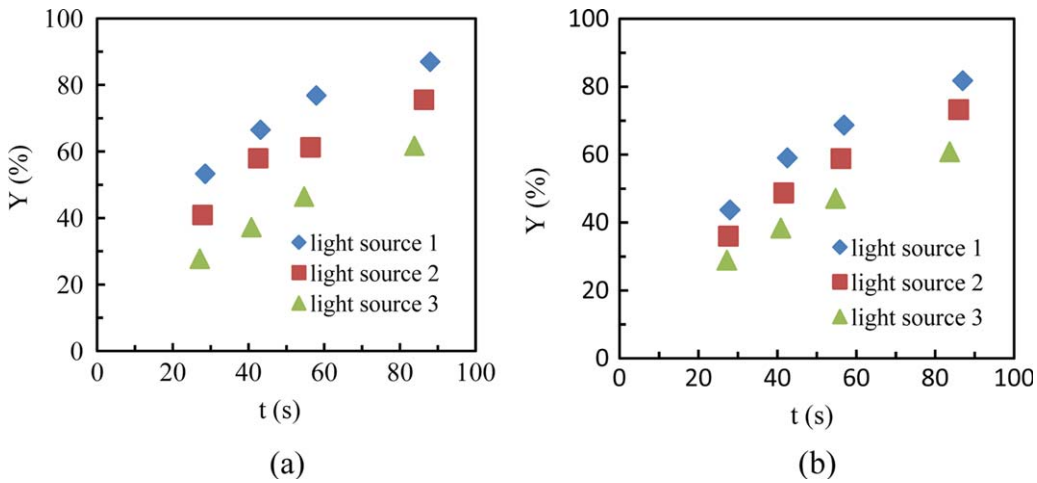

Figure 6. Effect of LED light sources on the yield.

(a) 1% Eosin Y loading and 1 equivalent TMEDA; (b) 0.25% Eosin Y loading and 1 equivalent TMEDA. [Color figure can be viewed in the online issue, which is available at wileyonlinelibrary.com.]

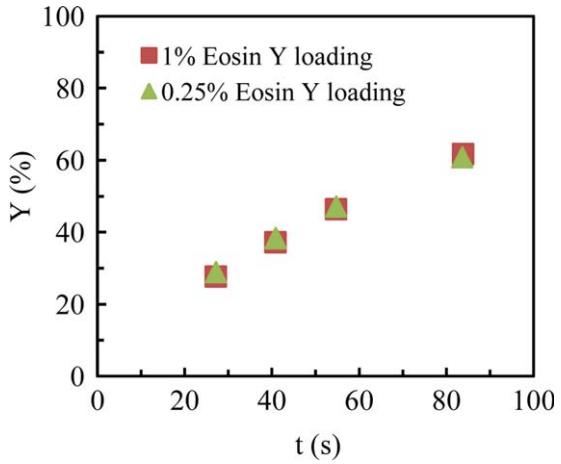

Figure 7. Effect of photocatalyst loading on the yield at light source 3 (1 equivalent TMEDA).

[Color figure can be viewed in the online issue, which is available at wileyonlinelibrary.com.]

Gas-liquid photocatalytic reaction kinetic analysis

Reaction Order with Respect to Substrate (thiophenol). Integration and differentiation methods are the two main approaches to deal with experimental data when studying reaction kinetics. In particular, the integration method is applicable to reaction processes in which the conversion of reactants is relatively high. As discussed above, the mass transfer limitation was completely overcome when the photochemical processes were carried out in Zone 1 using pure oxygen. In this case, the oxygen concentration in the reaction mixture approximately maintained the same value and was equal to the saturated concentration of oxygen in ethanol.

Two assumptions, including the first order reaction and the second order reaction with respect to the substrate, were made using the integration method. If the photocatalytic reaction is first order with respect to thiophenol (case 1), the reaction rate of substrate can be expressed as follows

$$r_{sub} = -\frac{dC_{sub}}{dt} = K_{sub,1} C_{sub} \tag{4}$$

$$\ln\left(\frac{C_{sub,0}}{C_{sub}}\right) = \ln\left(\frac{C_{sub,0}}{C_{sub,0}(1-X_{sub})}\right) = \ln\left(\frac{C_{sub,0}}{C_{sub,0}(1-Y)}\right) = K_{sub,1} t \tag{5}$$

where $K_{sub,1}$ is the apparent reaction rate constant with regard to thiophenol in case 1. The value of $K_{sub,1}$ includes information on the intrinsic reaction rate constant, the concentration of oxygen in the bulk liquid phase and the LED illumination. The yield (Y) is equal to the conversion (X_{sub}) due to the fact that the selectivity of phenyl disulfide is 100%. We observed no overoxidation, which demonstrates the mildness of this photocatalytic protocol. If the reaction is second order with respect to the substrate (case 2), the reaction rate is given by the following equations

$$r_{sub} = -\frac{dC_{sub}}{dt} = K_{sub,2} C_{sub}^2 \tag{6}$$

$$\frac{1}{C_{sub,0}(1-Y)} - \frac{1}{C_{sub,0}} = K_{sub,2} t \tag{7}$$

where $K_{sub,2}$ is the apparent reaction rate constant with regard to thiophenol in case 2. Figure 8 shows the validation of these two assumptions. It can be seen that the experimental data can be well explained based on the assumption of case 1 (Figure 8a); the linear correlation coefficient for the relationship between $\ln(C_{sub,0}/C_{sub})$ and the reaction time (residence time) is more than 0.99 (Figure 8a). However, the experimental data cannot be elaborated with the assumption of case 2 (Figure 8b). Based on this fundamental analysis, it can be concluded that the photocatalytic aerobic oxidation of thiophenol to phenyl disulfide is first order with respect to thiophenol. In addition, the apparent reaction rate constant (K_{sub}) can be directly obtained from the slope in Figure 8a, which can be used to calculate the intrinsic reaction rate constant.

Reaction Order with Respect to Oxygen. Oxygen is one of reactants in this photocatalytic oxidation process, and its role as oxidant is of vital importance. Therefore, the investigation of its reaction order will be beneficial for a further understanding of the reaction mechanism and its role in the photocatalytic process.

Keeping the conversion of thiophenol low and thus its concentration close to a constant value is mandatory when

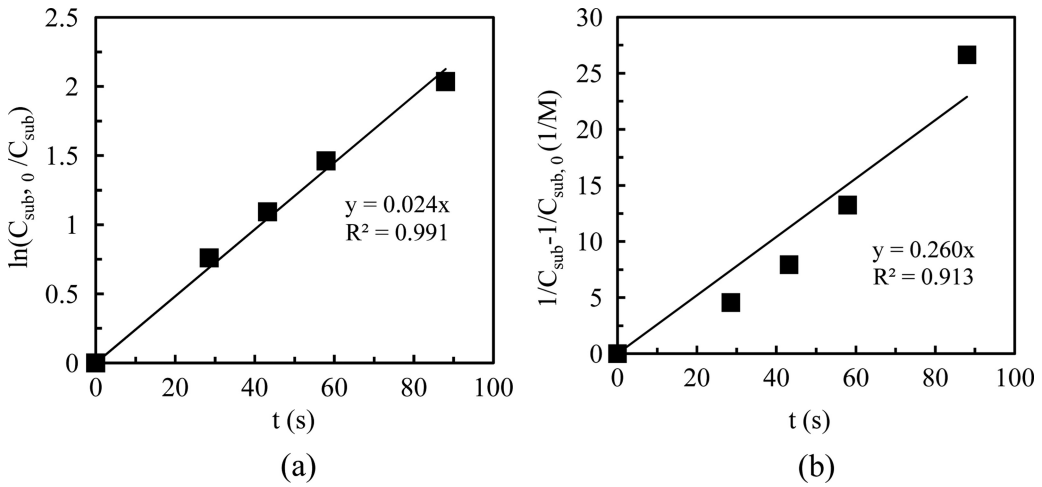

Figure 8. Validation of the reaction order with respect to the substrate in the gas-liquid photochemical catalysis (1% Eosin Y loading, 1 equivalent TMEDA and light source 1).

(a) case 1: first order; (b) case 2: second order.

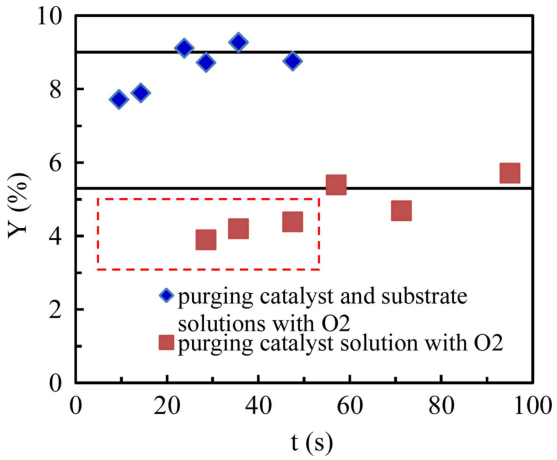

Figure 9. The yield versus the reaction time for two different cases in the homogeneous reaction process (1 equivalent TMEDA and light source 1; blue points: 0.25% Eosin Y loading; red points: 1% Eosin Y loading).

[Color figure can be viewed in the online issue, which is available at wileyonlinelibrary.com.]

applying the integration method. Minor variations on the experimental procedure were made in order to achieve this goal. Instead of introducing the gas phase (pure oxygen) into the capillary microreactor, we purged the substrate solution and/or the catalyst solution with pure oxygen for about 3 min before introducing the saturated solution into the capillary microreactor. Figure 9 shows the experimental results obtained for these homogeneous reactions. It can be seen that the yield first increased and then stabilized at a certain value in both cases. The mixing efficiency in microchannels or microcapillaries increases with increasing fluid flow rate for homogeneous mixing processes.[47,48] In other words, the decrease of residence time results in a higher mixing efficiency, which makes the reaction to be kinetically controlled instead of mixing controlled. As can be seen from Figure 9, the conversion of thiophenol was still too high when both substrate and catalyst solutions were purged with oxygen, even though the catalyst was lowered to 0.25 mol%. These results indicate the high dependence of the reaction rate on the oxygen concentration. However, when only the catalyst solution was purged, suitable data for kinetic analysis was obtained (see red frame in Figure 9). In addition, the original concentration of oxygen in the reaction mixture can be back-calculated based on the maximum yield

$$C_{O_2,0}=\frac{1}{4}C_{sub,0}X_{max}=\frac{1}{4}C_{sub,0}Y_{max} \tag{8}$$

Again, two assumptions were made to obtain the reaction order with respect to oxygen. If the reaction is first order (case A), the following equations can be obtained, which include the known reaction order for thiophenol

$$r_{O_2}=-\frac{dC_{O_2}}{dt}=k_{O_2}C_{sub}C_{O_2}=k_{O_2,A}C_{sub,0}C_{O_2}=K_{O_2,A}C_{O_2} \tag{9}$$

$$\ln\left(\frac{C_{O_2,0}}{C_{O_2}}\right)=\ln\left(\frac{C_{O_2,0}}{C_{O_2,0}-1/4YC_{sub,0)}}\right)=K_{O_2,A}t \tag{10}$$

$$r_{sub}=k_{sub,A}C_{sub}C_{O_2} \tag{11}$$

$$k_{sub,A}=4k_{O_2,A} \tag{12}$$

where $k_{O_2,A}(k_{O_2,A})$ and $k_{sub,A}(k_{sub,A})$ are the intrinsic / apparent reaction rate constants with regard to oxygen and thiophenol in case A, respectively. If the reaction is second order with respect to the oxygen concentration (case B), the reaction rate of oxygen consumption can be expressed as follows

$$r_{O_2}=-\frac{dC_{O_2}}{dt}=k_{O_2,B}C_{sub}C_{O2}{}^2=k_{O_2,B}C_{sub,0}C_{O_2}{}^2=K_{O_2,B}C_{O_2}{}^2 \tag{13}$$

$$\frac{1}{C_{O_2}}-\frac{1}{C_{O_2,0}}=\frac{1}{C_{O_2,0}-1/4YC_{sub,0}}-\frac{1}{C_{O_2,0}}=K_{O_2,B}t \tag{14}$$

$$r_{sub}=k_{sub,B}C_{sub}C_{O_2}{}^2 \tag{15}$$

$$k_{sub,B}=4k_{O_2,B} \tag{16}$$

where $k_{O_2,B}(k_{O_2,B})$ and $k_{sub,B}(k_{sub,B})$ are respectively the intrinsic/apparent reaction rate constants with regard to

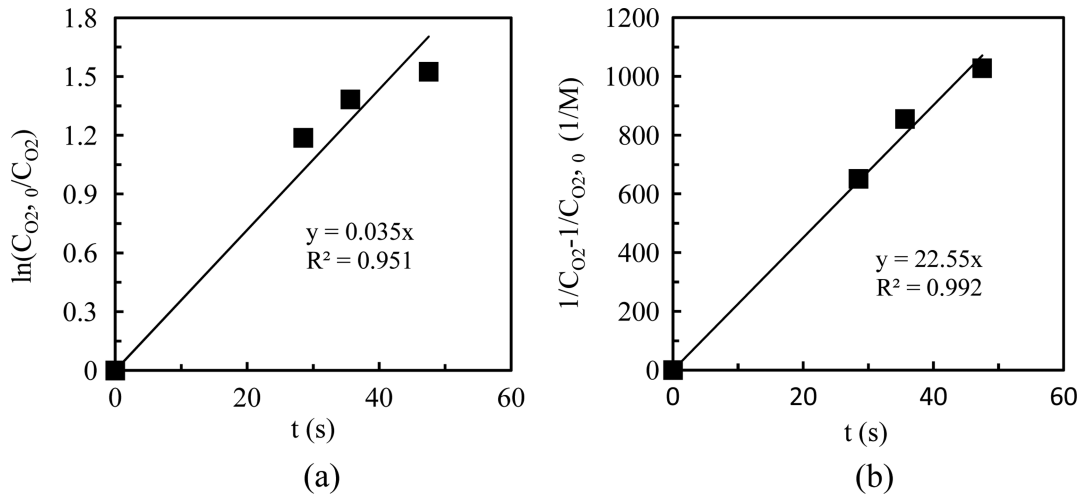

Figure 10. Validation of the reaction order with respect to oxygen in the homogeneous reaction process (1% Eosin Y loading, 1 equivalent TMEDA and light source 1).

(a) case A: first order; (b) case B: second order.

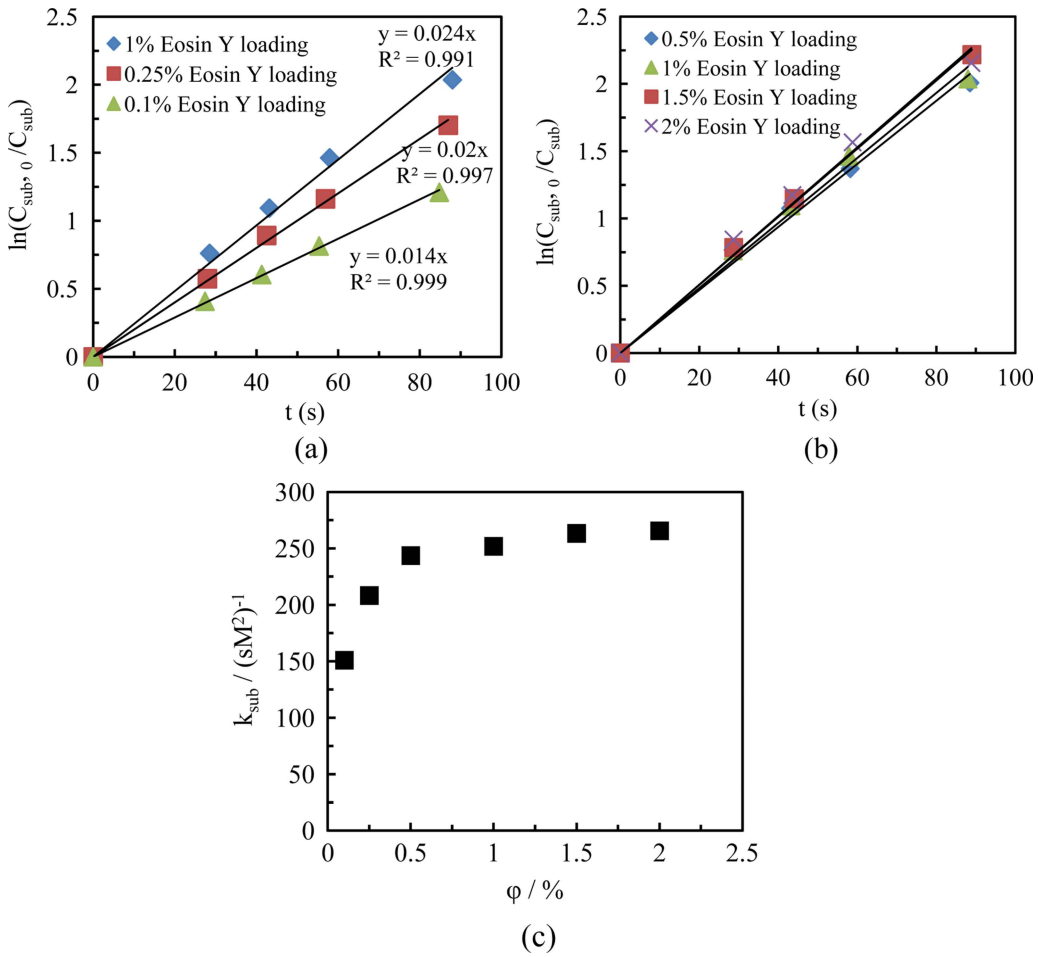

Figure 11. Handling of experimental data and corresponding kinetic results for different photocatalyst loadings (1 equivalent TMEDA and light source 1).

(a) the relationship between $\ln(C_{sub,0}/C_{sub})$ and t; (b) the relationship between $\ln(C_{sub,0}/C_{sub})$ and t with Eosin Y loading higher than 0.5%; (c) the relationship between the reaction rate constant and the Eosin Y loading. [Color figure can be viewed in the online issue, which is available at wileyonlinelibrary.com.]

oxygen and thiophenol in case B. These two assumptions (case A and case B) are examined in Figure 10. It can be seen that the relationship between $(1/C_{O_2}-1/C_{O_2,0})$ and the reaction time is strictly linear with a correlation coefficient more than 0.99 for the second order assumption (Figure 10b). Therefore, the assumption of case B is reasonable and this aerobic photocatalytic oxidation of thiophenol to phenyl disulfide is second order in oxygen.

Furthermore, the reaction rate constants obtained from both the gas-liquid heterogeneous reaction and the homogeneous reaction are compared. For the homogeneous process, the reaction rate constants for oxygen and thiophenol can be obtained as follows

$$k_{O_2,homo}=\frac{K_{O_2,B}}{C_{sub,0}}=90(sM^2)^{-1} \tag{17}$$

$$k_{sub,homo}=4k_{O_2,homo}=360(sM^2)^{-1} \tag{18}$$

The reaction rate constant for thiophenol can be calculated from the heterogeneous process as follows

$$k_{sub,hete}=\frac{K_{sub,1}}{C^{*2}_{O_2}}=252(sM^2)^{-1} \tag{19}$$

$$[k_{sub,hete}=252(sM^2)^{-1}]<[k_{sub,homo}=360(sM^2)^{-1}] \tag{20}$$

The reaction rate constants with regard to substrate for the homogeneous and heterogeneous photocatalytic processes are in the same magnitude, which further demonstrates the rationality of the assumptions for case 1 and case B. The lower value of reaction rate constant in the heterogeneous process may be related to light-scattering phenomena, which are often involved in multiphase operations during photochemical transformations.[57]

Supposing the assumption of case A was tenable, the following inequality can be obtained

$$\left[k_{sub,hete}=2.5(sM)^{-1}\right]\gg\left[k_{sub,homo}=0.57(sM)^{-1}\right] \tag{21}$$

The reaction rate constants for the homogeneous and heterogeneous processes are not in the same order of magnitude and show a large deviation between them. This reasoning further excludes the rationality of case A (Figure 10a).

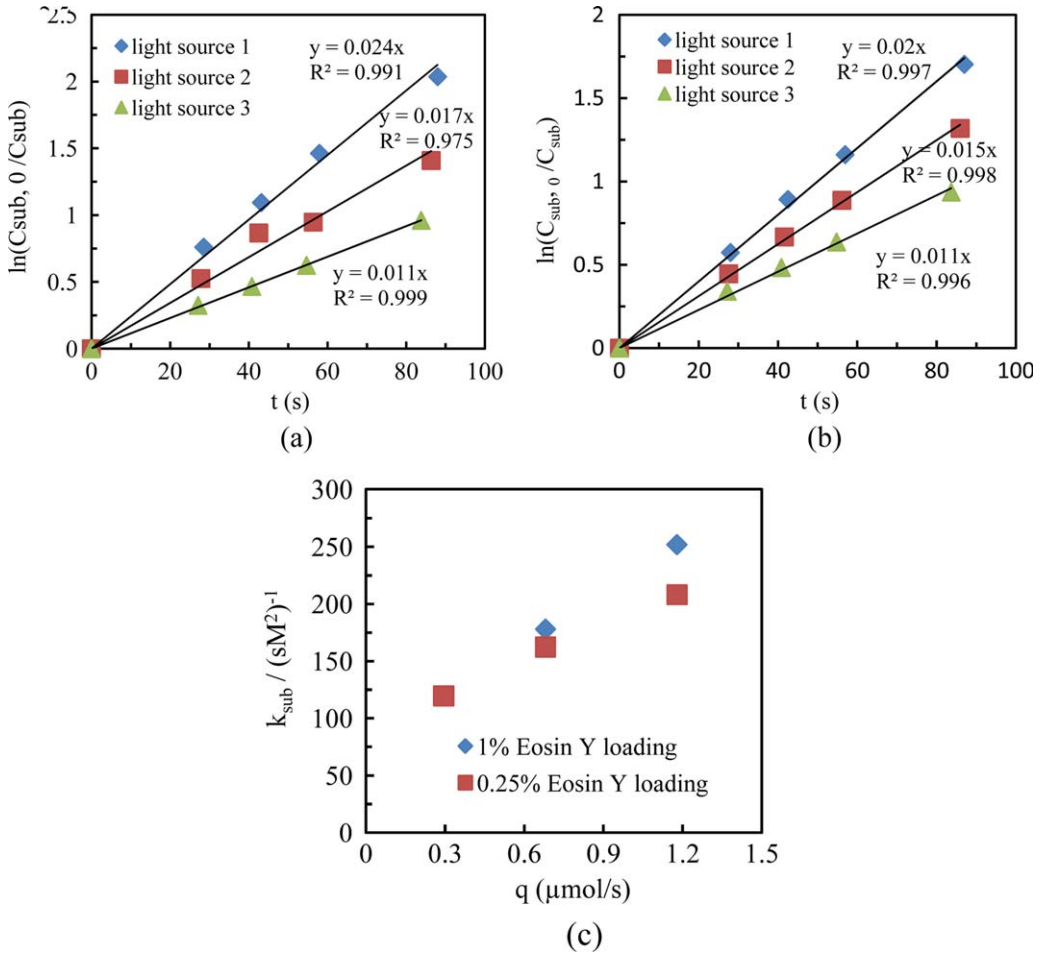

Figure 12. (a) The relationship between $\ln(C_{sub,0}/C_{sub})$ and t with 1 equivalent TMEDA for 1% Eosin Y loading; (b) for 0.25% Eosin Y loading; (c) the variation of reaction rate constant with the photon flux (c).

[Color figure can be viewed in the online issue, which is available at wileyonlinelibrary.com.]

With the known reaction rate constants in hand, now the Hatta number for the photocatalytic aerobic oxidation can be calculated according to its definition

$$Ha = \frac{\sqrt{\frac{2}{m+1}k_{O_2,\text{hete}}(c_{O_2,\text{in}})^{m-1}(c_{\text{sub,L}})^{n}D_{O_2}}}{k_L} = \frac{\sqrt{\frac{2}{3}k_{O_2,\text{hete}}(C^{*}_{O_2})^{1}(c_{\text{sub,L}})^{1}D_{O_2}}}{k_L} \quad (22)$$

where m and n are respectively the reaction orders for oxygen and thiophenol, and k_L is the liquid side mass transfer coefficient. The value of k_L is about 2.6×10^{-4} m/s when the volumetric flow rates of 900 μL/min (gas phase) and 300 μL/min (liquid phase) are applied in the capillary microreactor.[53–55] The value of Ha number is then obtained ($Ha = 0.06$), which is obviously lower than 3 and even lower than 0.3. This low value of Ha number means that the photocatalytic reaction did not occur in the gas-liquid interface and its very adjacent zones (c.f., liquid film zone),[58] but it occurred in the bulk liquid phase due to the fast mass transfer rate of oxygen provided by gas-liquid Taylor flow within the capillary microreactor. The value of Ha also indicates the elimination of mass transfer limitations in the reaction kinetic study.

Reaction Rate Constants with Different Photocatalyst Loadings. Figure 11 shows the handling of experimental data and corresponding kinetic results at different photocatalyst loadings. It can be seen that the reaction rate constant significantly increased with increasing Eosin Y loading up to 0.5% loading. A further increase in the Eosin Y loading did not evidently increase the reaction rate constant and thus the reaction performance.

Reaction Rate Constants with Different Photon Flux. Various light sources have different spectral characteristics, generating different light intensity and photon flux distribution. By integrating the photon flux distribution (Figure 2a) in this wavelength range, we can obtain the effective flux of photons that may be absorbed by the reaction mixture during the photocatalytic process. Figure 12 shows the relationship between $\ln(C_{sub,0}/C_{sub})$ and t for two Eosin Y loadings and the variation of the reaction rate constant at different photon fluxes. It can be seen that the photon flux affects the reaction rate constant remarkably, especially at high photocatalyst loadings. The effect of the photocatalyst loading amount on the reaction rate constant was relatively weak at low photon fluxes. The reaction activity can be high under the excitation with high photon flux even when the photocatalyst loading is low. Therefore, the photocatalyst loading and the light source should match each other when optimizing a

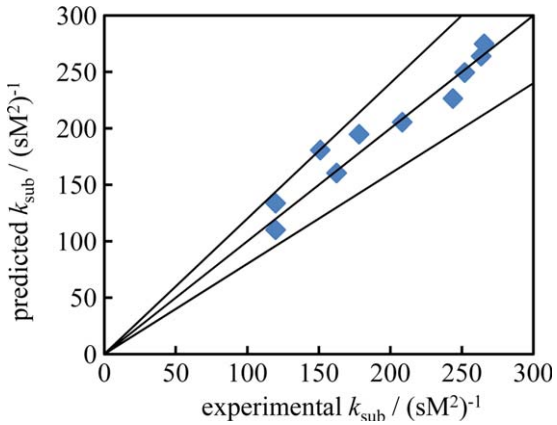

Figure 13. Experimental values of reaction rate constants vs. predicted values.

[Color figure can be viewed in the online issue, which is available at wileyonlinelibrary.com.]

photocatalytic process. The following correlation based on the multiple linear regression analysis can approximately describe the relative importance of photon flux and photocatalyst loading in this gas-liquid photocatalytic oxidation (q: 0.29–1.18 μmol/s; φ: 0.25–2%)

$$k_{sub}=228.6q^{0.56}\varphi^{0.21} \tag{23}$$

Figure 13 shows that relative deviations between the experimental and predicted values of reaction rate constants are in the range of −20 – 20% by Eq. 23.

Comparison between continuous-flow and batch processing

A glass test tube (ID: 10 mm) connected with an oxygen balloon was used to investigate the photocatalytic aerobic oxidation of thiophenol in batch. In this reactor vessel, 1 or 2 mL reaction solution (0.25 M thiophenol, 1 mol% Eosin Y, and 1 equivalent TMEDA in the ethanol) was agitated with a small magnetic stirrer. The reaction mixture was irradiated by light source 1. Figure 14 shows the effect of the stirring rate on the yield in function of time. It can be seen that the yield significantly increased with an increase of the stirring rate. This indicates that gas-liquid mass transfer limitations indeed occur in batch experiments. Moreover, the yield for the 2 mL reaction mixture was lower than the one obtained in a 1 mL experiment indicating again that mass transfer limitations dominate the photocatalytic process. The mean rate of mechanical energy dissipation (ε_{av}) for the 2 mL reaction mixture with the stirring rate of 1150 revolutions per minute (rpm) was kept the same as for the 1 mL reaction mixture with the stirring rate of 900 rpm, according to the following equation[58]

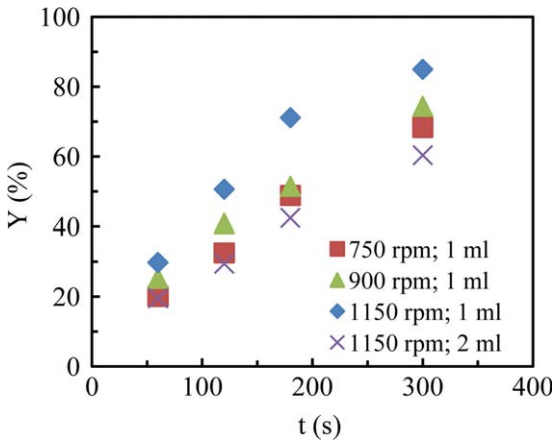

Figure 14. Effect of stirring rate on the yield in the batch processing (1% Eosin Y loading, 1 equivalent TMEDA and light source 1).

[Color figure can be viewed in the online issue, which is available at wileyonlinelibrary.com.]

$$\varepsilon_{av}=P/(\rho V)=P_oN^3d^5/V \tag{24}$$

where d is the stirrer diameter, V is the liquid volume, N is the rotational stirring speed, P is the power consumption of the stirrer, P_o is the power number (dimensionless parameter, depending on the stirrer type), and ρ is the liquid density. The obviously lower yield for 2 mL reaction mixture indicated the low mechanical energy utilization and the challenging scale-up of batch reactors, partly arising from the low mass transfer rate.

Next, the apparent reaction rate constant of thiophenol was calculated for the 1 mL reaction mixture with the stirring rate of 1150 rpm; its value was 66.6 M^{-2} s^{-1}. It was much lower than the intrinsic reaction rate constant (252 M^{-2} s^{-1}) obtained from the continuous-flow processing using the same light source. The mass transfer rate of oxygen from the gas phase to the liquid phase was low in the batch reactor due to its low surface-to-volume ratio. The dependence of reaction rate on the oxygen concentration is rather strong, in which the second order relation can be found according to the reaction kinetic equation. On the other hand, the characteristic dimension of this small batch reactor (test tube) for photon transport was still much larger than the capillary microreactor, resulting in an inhomogeneous irradiation of the reaction mixture.

Conclusions

We have developed a compact and operationally simple photomicroreactor assembly that consists of a capillary microreactor and small-scale LEDs. The reaction kinetics of gas-liquid photocatalytic aerobic oxidation of thiophenol to phenyl disulfide was studied in this device. A fast consumption of gaseous reactant (oxygen) was observed upon irradiation of the reaction mixture with LED light. We have described the mass transfer of oxygen from the gas to the liquid phase during the photocatalytic process in detail. Mass transfer limitations were eliminated by selecting an appropriate operational zone with regard to the volumetric flow rate ratio of gas-to-liquid phase.

Reaction kinetic analysis was performed in order to understand the key influencing parameters for gas-liquid aerobic photocatalytic processes. The reaction orders with respect to thiophenol and oxygen were found to be 1 and 2, respectively. The value of the Hatta number, that is, $Ha = 0.06$, indicated that the mass transfer limitation was indeed eliminated and the reaction only occurred in the bulk liquid phase in our photochemical column. In addition, the extreme low value of Ha demonstrates the potential application of this kind of photochemical columns for reaction kinetic studies of other unique gas-liquid photocatalytic reactions in which the intrinsic kinetics is ultimately fast.

The reaction rate constants were obtained at different photocatalyst loadings and different photon flux. Faster reactions were observed with an increase of photocatalyst loading and photon flux. The reaction rate constant obtained in the photochemical column was much higher than the one obtained in a batch reactor. Given the low cost prize of our photochemical column, we anticipate that our photochemical column will find broad application in academia and industry.

Acknowledgments

Y.S. would like to thank the European Union for a Marie Curie—Intra-European Fellowship (No 622415). T.N. would like to acknowledge financial support from the Dutch Science Foundation for a VENI Grant (No 12464) and from the European Union for a Marie Curie CIG Grant (Grant No. 333659).

Literature Cited

1. Chatani S, Kloxin CJ, Bowman CN. The power of light in polymer science: photochemical processes to manipulate polymer formation, structure, and properties. *Polym Chem*. 2014;5:2187–2201.
2. Smestad GP, Steinfeld A. Review: photochemical and thermochemical production of solar fuels from H2O and CO2 using metal oxide catalyst. *Ind Eng Chem Res*. 2012;51:11828–11840.
3. Bach T, Hehn JP. Photochemical reactions as key steps in natural product synthesis. *Angew Chem Int Ed*. 2011;50:1000–1045.
4. Hoffmann N. Photochemical reactions as key steps in organic synthesis. *Chem Rev*. 2008;108:1052–1103.
5. Alfano OM, Bahnemann D, Cassano AE, Dillert R, Goslich R. Photocatalysis in water environments using artificial and solar light. *Catal Today*. 2000;58:199–230.
6. Prier CK, Rankic DA, MacMillan DWC. Visible light photoredox catalysis with transition metal complexes: applications in organic synthesis. *Chem Rev*. 2013;113:5322–5363.
7. Ravelli D, Fagnoni M, Albini A. Photoorganocatalysis. *What for? Chem Soc Rev*. 2013;42:97–113.
8. Narayanam JMR, Stephenson CRJ. Visible light photoredox catalysis: applications in organic synthesis. *Chem Soc Rev*. 2011;40:102–113.
9. Cassano AE, Martin CA, Brandi RJ, Alfano OM. Photoreactor analysis and design: fundamentals and applications. *Ind Eng Chem Res*. 1995;34:2155–2201.
10. Colina-Márquez J, Machuca-Martínez F, Puma GL. Radiation absorption and optimization of solar photocatalytic reactors for environmental applications. *Environ Sci Technol*. 2010;44:5112–5120.
11. Lévesque F, Seeberger PH. Highly efficient continuous flow reactions using singlet oxygen as a "Green" reagent. *Org Lett*. 2011;13:5008–5011.
12. Carofiglio T, Donnola P, Maggini M, Rossetto M, Rossi E. Fullerene-promoted singlet-oxygen photochemical oxygenations in glass-polymer microstructured reactors. *Adv Synth Catal*. 2008;350:2815–2822.
13. DeRosa MC, Crutchley RJ. Photosensitized singlet oxygen and its applications. *Coordin Chem Rev*. 2002;233-234:351–371.
14. Wootton RCR, Fortt R, deMello AJ. A microfabricated nanoreactor for safe, continuous generation and use of singlet oxygen. *Org Process Res Dev*. 2002;6:187–189.
15. Wang X, Cuny GD, Noël T. A mild, one-pot Stadler–Ziegler synthesis of arylsulfides facilitated by photoredox catalysis in batch and continuous-flow. *Angew Chemie Int Ed*. 2013;52:7860–7864.
16. Bremus-Kobberling E, Gillner A, Avemaria F, Rethore C, Brase S. Photochemistry with laser radiation in condensed phase using miniaturized photoreactors. *Beilstein J Org Chem*. 2012;8:1213–1218.
17. Su Y, Chen G, Kenig EY. An experimental study on the numbering-up of microchannels for liquid mixing. *Lab Chip*. 2015;15(1):179–187.
18. Al-Rawashdeh M, Yue F, Patil NG, Nijhuis TA, Hessel V, Schouten JC, Rebrov EV. Designing flow and temperature uniformities in parallel microchannels reactor. *AIChE J*. 2014;60:1941–1952.
19. McQuade DT, Seeberger PH. Applying flow chemistry: methods, materials, and multistep synthesis. *J Org Chem*. 2013:78,6384–6389.
20. Hessel V, Kralisch D, Kockmann N, Noël T, Wang Q. Novel process windows for enabling, accelerating, and uplifting flow chemistry. *ChemSusChem*. 2013;6:746–789.
21. Kashid MN, Renken A, Kiwi-Minsker L. Gas–liquid and liquid–liquid mass transfer in microstructured reactors. *Chem Eng Sci*. 2011;66:3876–3897.
22. Noël T, Buchwald SL. Cross-coupling in flow. *Chem Soc Rev*. 2011;40:5010–5029.
23. Chen G, Yue J, Yuan Q. Gas-liquid microreaction technology: recent developments and future challenges. *Chinese J Chem Eng*. 2008;16:663–669.
24. Wang K, Lu YC, Xu JH, Gong XC, Luo GS. Reducing side product by enhancing mass-transfer rate. *AIChE J*. 2006;52 (12):4207–4213.
25. Aillet T, Loubière K, Prat L, Dechy-Cabaret O. Impact of the diffusion limitation in microphotoreactors. *AIChE J*. 2015;61:1284–1299.
26. Su Y, Straathof NJW, Hessel V, Noël T. Photochemical transformations accelerated in continuous-flow reactors: basic concepts and applications. *Chem—A Eur J*. 2014;20:10562–10589.
27. Noël T, Wang X, Hessel V. Accelerating photoredox catalysis in continuous microflow. *Chim Oggi*. 2013;31:10–14.
28. Oelgemoeller M. Highlights of photochemical reactions in microflow reactors. *Chem Eng Technol*. 2012;35:1144–1152.
29. Knowles JP, Elliott LD, Booker-Milburn KI. Flow photochemistry: old light through new windows. *Beilstein J Org Chem*. 2012;8:2025–2052.
30. Aillet T, Loubiere K, Dechy-Cabaret O, Prat L. Photochemical synthesis of a "cage" compound in a microreactor: rigorous comparison with a batch photoreactor. *Chem Eng Process*. 2013;64:38–47.
31. Bachollet S, Terao K, Aida S, Nishiyama Y, Kakiuchi K, Oelgemoeller M. Microflow photochemistry: UVC-induced [2+ 2]-photoadditions to furanone in a microcapillary reactor. *Beilstein J Org Chem*. 2013;9:2015–2021.
32. Terao K, Nishiyama Y, Tanimoto H, Morimoto T, Oelgemoeller M. Diastereoselective [2+ 2] photocycloaddition of a chiral cyclohexenone with ethylene in a continuous flow microcapillary reactor. *J Flow Chem*. 2012;2:73–76.
33. Straathof NJW, Gemoets HPL, Wang X, Schouten JC, Hessel V, Noël T. Rapid trifluoromethylation and perfluoroalkylation of five-membered heterocycles by photoredox catalysis in continuous flow. *ChemSusChem*. 2014:7:1612–1617.
34. Straathof NJW, van Osch DJGP, Schouten A, Wang X, Schouten JC, Hessel V, Noël T. Visible light photocatalytic metal-free perfluoroalkylation of heteroarenes in continuous flow. *J Flow Chem*. 2014;4:12–17.
35. Levesque F, Seeberger PH. continuous-flow synthesis of the anti-malaria drug artemisinin. *Angew Chem Int Ed*. 2012;51:1706–1709.
36. Park CP, Maurya RA, Lee J H, Kim DP. Efficient photosensitized oxygenations in phase contact enhanced microreactors. *Lab Chip*. 2011;11:1941–1945.
37. Jähnisch K, Dingerdissen U. Photochemical generation and [4+ 2]-cycloaddition of singlet oxygen in a falling-film micro reactor. *Chem Eng Technol*. 2005;28:426–427.
38. Meyer S, Tietze D, Rau S, Schäfer B, Kreisel G. Photosensitized oxidation of citronellol in microreactors. *J Photochem Photobiol A Chem*. 2007;186:248–253.
39. Elvira KS, Wootton RCR, Reis NM, Mackley MR, deMello AJ. Through-wall mass transport as a modality for safe generation of singlet oxygen in continuous flows. *ACS Sustainable Chem Eng*. 2013:1:209–213.
40. Vaidya PD, Kenig EY. Gas–Liquid reaction kinetics: a review of determination methods. *Chem Eng Commun*. 2007;194:1543–1565.
41. Ye C, Dang M, Yao C, Chen G, Yuan Q. Process analysis on CO_2 absorption by monoethanolamine solutions in microchannel reactors. *Chem Eng J*. 2013;225:120–127.
42. Li W, Liu K, Simms R, Greener J, Jagadeesan D, Pinto S, Günther A, Kumacheva E. Microfluidic study of fast gas–liquid reactions. *J Am Chem Soc*. 2012;134:3127–3132.
43. Keybl J, Jensen KF. Microreactor system for high-pressure continuous flow homogeneous catalysis measurements. *Ind Eng Chem Res*. 2011;50:11013–11022.
44. Talla A, Driessen B, Straathof NJW, Milroy LG, Brunsveld L, Hessel V, Noël T. Metal-free photocatalytic aerobic oxidation of thiols to disulfides in batch and continuous-flow. *Adv Synth Catal*. 2015, DOI: 10.1002/adsc.201401010.
45. Trivedi MV, Laurence JS, Siahaan TJ. The role of thiols and disulfides in protein chemical and physical stability. *Curr Prot Pept Sci*. 2009;10:614–625.
46. Laborie S, Cabassud C, Durand-Bourlier L, Lainé JM. Characterisation of gas-liquid two-phase flow inside capillaries. *Chem Eng Sci*. 1999;54:5723–5735.

47. Angeli P, Gavriilidis A. Hydrodynamics of Taylor flow in small channels: a review. *Proc Inst Mech Eng C- J Mech Eng Sci*. 2008; 222:737–751.
48. Tan J, Lu YC, Xu JH, Luo GS. Mass transfer characteristic in the formation stage of gas–liquid segmented flow in microchannel. *Chem Eng J*. 2012;185:314–320.
49. Sobieszuk P, Pohorecki R, Cygański P, Grzelka J. Determination of the interfacial area and mass transfer coefficients in the Taylor gas–liquid flow in a microchannel. *Chem Eng Sci*. 2011;66:6048–6056.
50. Yue J, Luo L, Gonthier Y, Chen G, Yuan Q. An experimental study of air–water Taylor flow and mass transfer inside square microchannel. *Chem Eng Sci*. 2009;64:3697–3708.
51. Hartman RL, McMullen JP, Jensen KF. Deciding whether to go with the flow: evaluating the merits of flow reactors for synthesis. *Angew Chem Int Ed*. 2011;50:7502–7519.
52. Kucka L, Richter J, Kenig EY, Górak A. Determination of gas–liquid reaction kinetics with a stirred cell reactor. *Sep Purif Technol*. 2003;31:163–175.
53. Su Y, Chen G, Yuan Q. Influence of hydrodynamics on liquid mixing during Taylor flow in a microchannel. *AIChE J*. 2012;58:1660–1670.
54. Garstecki P, Fuerstman MJ, Stone HA, Whitesides GM. Formation of droplets and bubbles in a microfluidic T-junction—scaling and mechanism of break-up. *Lab Chip*. 2006;6:437–446.
55. van Baten JM, Krishna R. CFD simulations of mass transfer from Taylor bubbles rising in circular capillaries. *Chem Eng Sci*. 2004;59: 2535–2545.
56. Hari DP, Konig B. Synthetic applications of eosin Y in photoredox catalysis. *Chem Commun*. 2014;50:6688–6699.
57. Pareek V, Chong S, Tadé M, Adesina AA. Light intensity distribution in heterogenous photocatalytic reactors. *Asia-Pac J Chem Eng*. 2008;3:171–201.
58. Bourne JR. Mixing and the selectivity of chemical reactions. *Org Process Res Dev*. 2003;7:471–508.

Manuscript received Nov. 19, 2014, and revision received Feb. 9, 2015.